

Electronic supplementary information (ESI) for

**Partially oxidized inter-doped RuNi alloy aerogel for the
hydrogen evolution reaction in both alkaline and acidic media**

Taehee Kim, Hwapyung Jung, Haryeong Choi, Wonjun Lee, Umakant M. Patil, Vinayak G. Parale, Younghun Kim, Jiseung Kim, Sang-Hyun Kim, and Hyung-Ho Park*

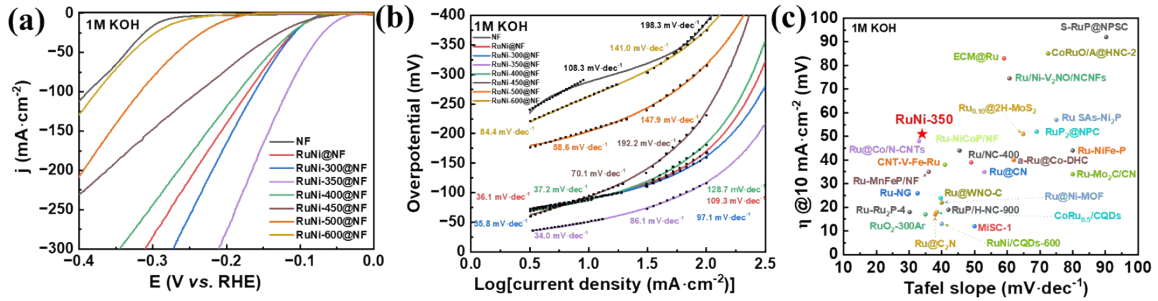


Figure S1. Comparison of the electrochemical HER activities of RuNi@NF with different oxidation temperature by (a) LSV curves and corresponding Tafel slopes (b) in alkaline electrolyte. (c) Comparison of HER performance in alkaline media (η at $10 \text{ mA}\cdot\text{cm}^{-2}$ and Tafel slope) for variously reported electrocatalysts. RuNi-350@NF is presented by a red star.

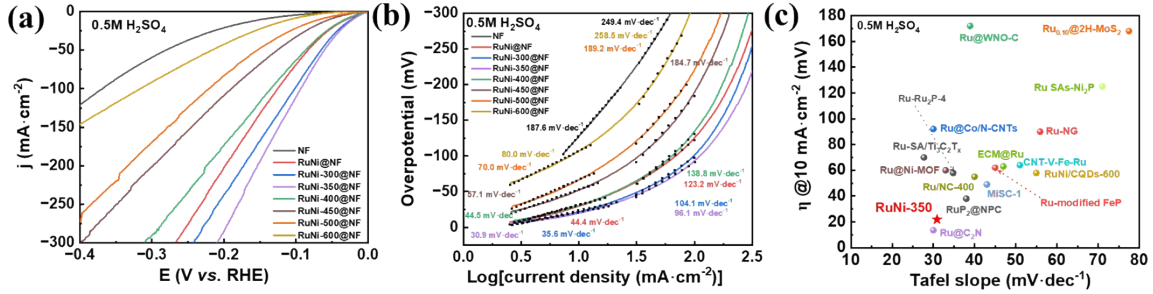


Figure S2. Comparison of the electrochemical HER activities of RuNi@NF with different oxidation temperature by (a) LSV curves and corresponding Tafel slopes (b) in acidic electrolyte. (c) Comparison of HER performance in acid media (η at $10 \text{ mA}\cdot\text{cm}^{-2}$ and Tafel slope) for variously reported electrocatalysts. RuNi-350@NF is presented by a red star.

Table S1. The calculated Tafel slopes at low and higher overpotentials for each samples

Samples	Acidic electrolyte		Alkaline electrolyte	
	1 st Tafel slope (mV·dec ⁻¹)	2 nd Tafel slope (mV·dec ⁻¹)	1 st Tafel slope (mV·dec ⁻¹)	2 nd Tafel slope (mV·dec ⁻¹)
NF	187.6	249.4	108.3	198.3
RuNi@NF	44.4	123.2	36.1	109.3
RuNi-300@NF	35.6	104.1	35.8	97.1
RuNi-350@NF	30.9	96.1	34.0	86.1
RuNi-400@NF	44.5	138.8	37.2	128.7
RuNi-450@NF	57.1	184.7	70.1	192.2
RuNi-500@NF	70.0	189.2	58.6	147.9
RuNi-600@NF	80.0	258.5	84.4	141.0

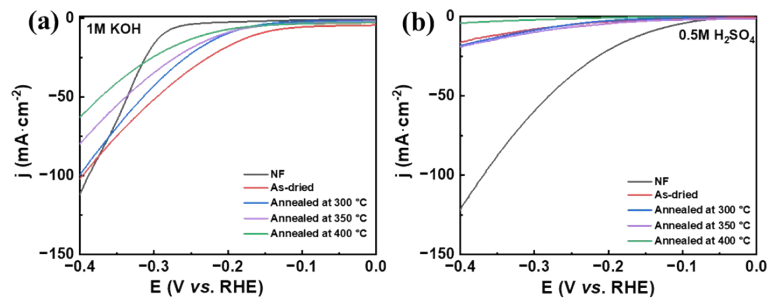


Figure S3. Comparison of the electrochemical HER activities of bare NF with supercritically dried and heat treated NF in (a) alkaline and (b) acidic media.

Table S2. Fitted electrical circuits and parameters of Nyquist plots of electrocatalysts (in KOH electrolyte)

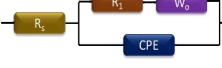
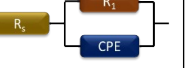
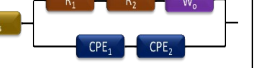
Parameters	RuNi@NF	RuNi-300@NF	RuNi-350@NF	RuNi-400@NF
R_s	0.1509	0.15011	0.15093	0.159
R_1	0.1901	0.16762	0.14375	0.0348
R_2	-	-	-	0.20024
W_{1-R}	0.18314	-	-	0.00015094
W_{1-T}	2.294	-	-	1.5234
W_{1-P}	0.021318	-	-	0.065604
CPE _{1-T}	0.027619	0.12802	0.1026	0.52684
CPE _{1-P}	0.62893	0.65982	0.67472	0.46534
CPE _{2-T}	-	-	-	0.020829
CPE _{2-P}	-	-	-	1.239
Chi-square value	0.00066	0.0010	0.0010	0.00051
Fitted Circuit				

Table S3. Fitted electrical circuits and parameters of Nyquist plots of electrocatalysts (in H₂SO₄ electrolyte)

Parameters	Ru@NF	Ru-300@NF	Ru-350@NF	Ru-400@NF
R _s	0.087104	0.094953	0.098034	0.086038
R ₁	0.21153	0.13477	0.08839	0.2484
CPE _{1-T}	0.041511	0.14794	0.055506	0.10597
CPE _{1-P}	0.5344	0.51928	0.63981	0.46486
Chi-square value	4.23 x 10 ⁻¹¹	2.11 x 10 ⁻⁵	3.12 x 10 ⁻⁵	1.0 x 10 ⁻⁵
Fitted Circuit				

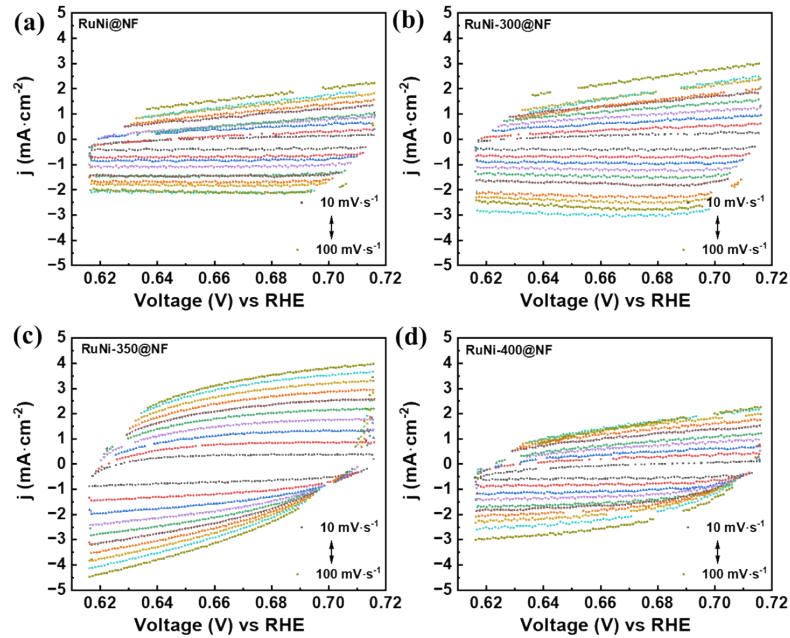


Figure S4. Cyclic voltammogram (CV) measured at non-Faradic region at various scan rates of (a) RuNi@NF, (b) RuNi-300@NF, (c) RuNi-350@NF, and (d) RuNi-400@NF.

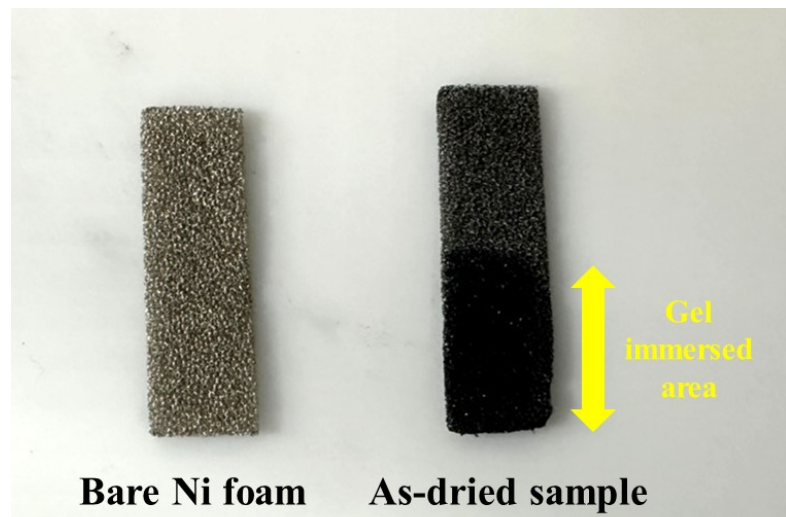


Figure S5. Optical images of bare nickel foam and after supercritical ethanol drying. The yellow arrow indicates areas where the gel has been applied and immersed.

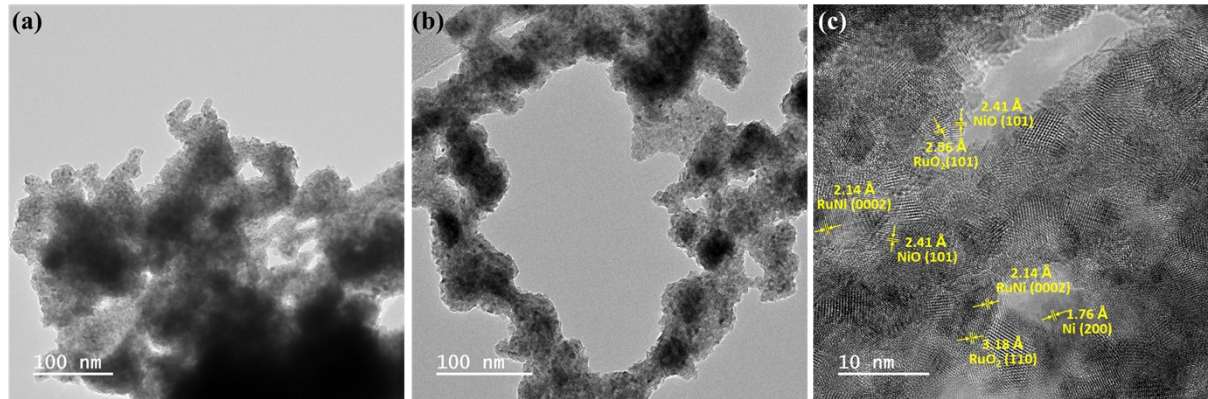


Figure S6. (a, b) TEM images and (c) a HRTEM image of the RuNi-350@NF indicating multipole phases.

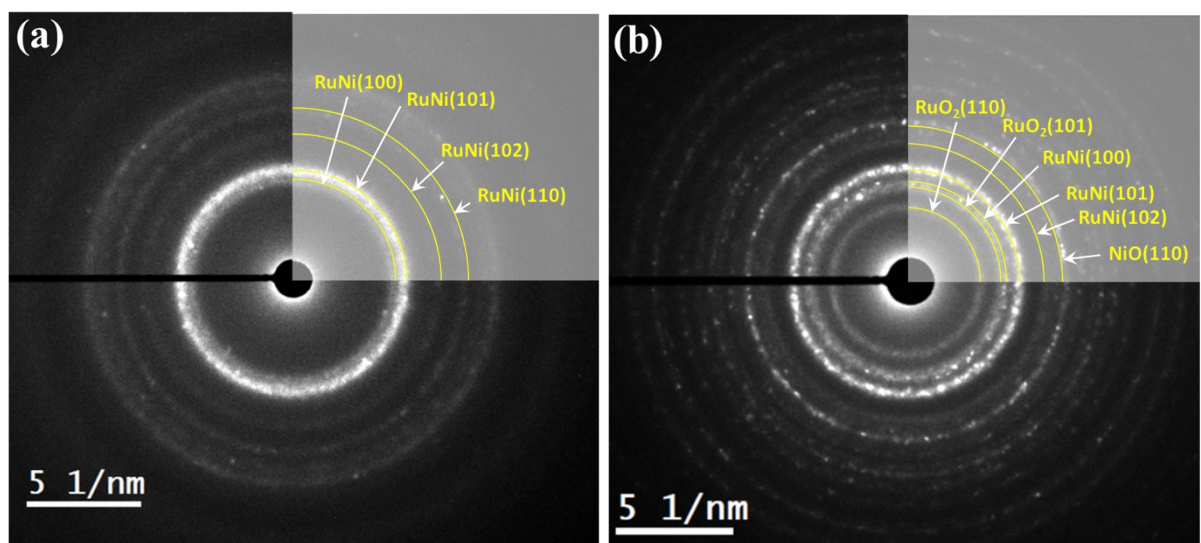


Figure S7. (a) SAED patterns of RuNi@NF and RuNi-350@NF samples representing the existence of multilayer phases.

Table S4. Chemical composition of each aerogel sample determined using EDX and STEM imaging

Element	RuNi (at%)	RuNi-300 (at%)	RuNi-350 (at%)	RuNi-400 (at%)
O	2.22	34.30	52.91	58.18
Ni	34.57	23.65	15.84	19.14
Ru	63.21	42.05	31.25	22.68
Total	100.00	100.00	100.00	100.00

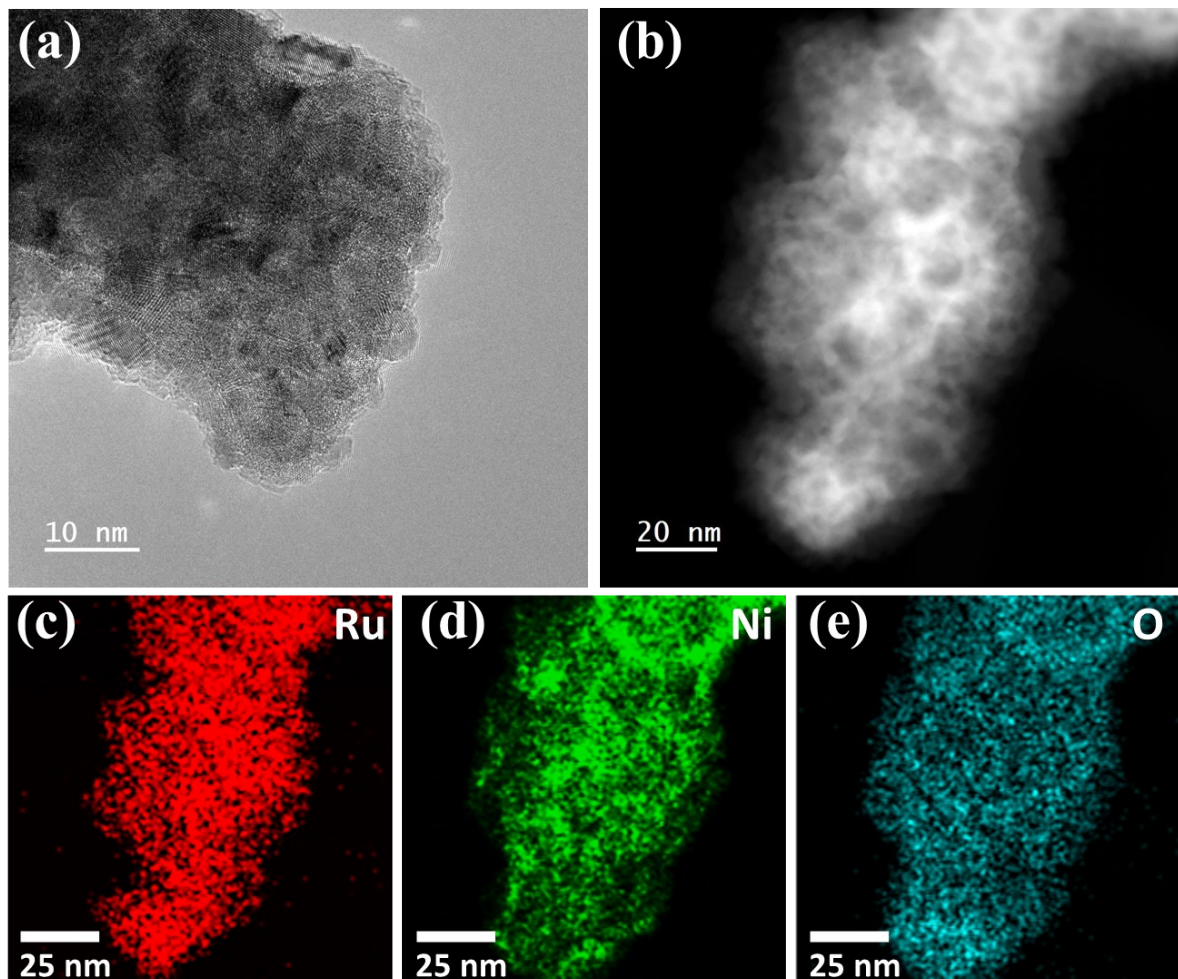


Figure S8. (a) HRTEM images of RuNi-300 aerogel, (b) HAADF-STEM image of RuNi-300 aerogel. EDX elemental mapping images of (c) Ru, (d) Ni, and (e) O in RuNi-300 aerogel catalyst.

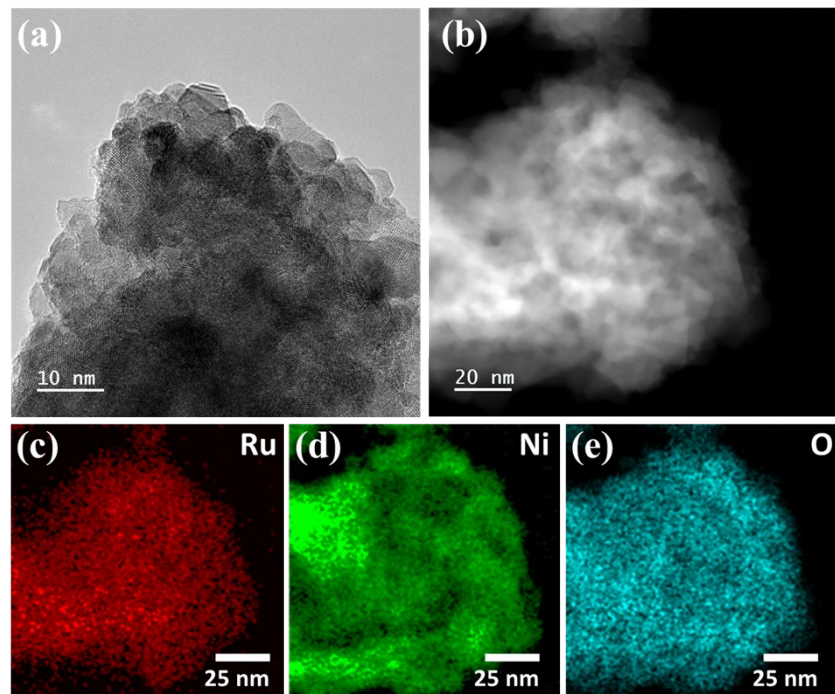


Figure S9. (a) HRTEM images of RuNi-400 aerogel, (b) HAADF-STEM image of RuNi-400 aerogel. EDX elemental mapping images of (c) Ru, (d) Ni, and (e) O in RuNi-400 aerogel catalyst.

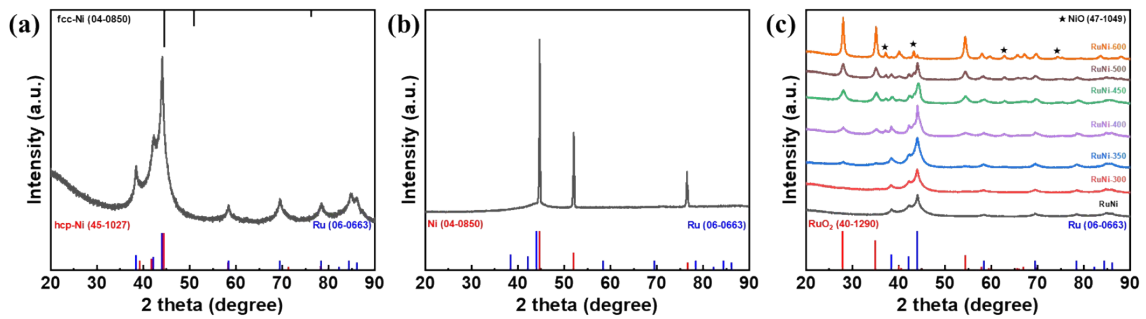


Figure S10. XRD patterns of (a) RuNi sample showing hcp-Ru and hcp-Ni phases, (b) RuNi@NF samples showing a strong peaks from NF and (c) aerogel samples with different oxidation temperatures from 300 to 600 °C.

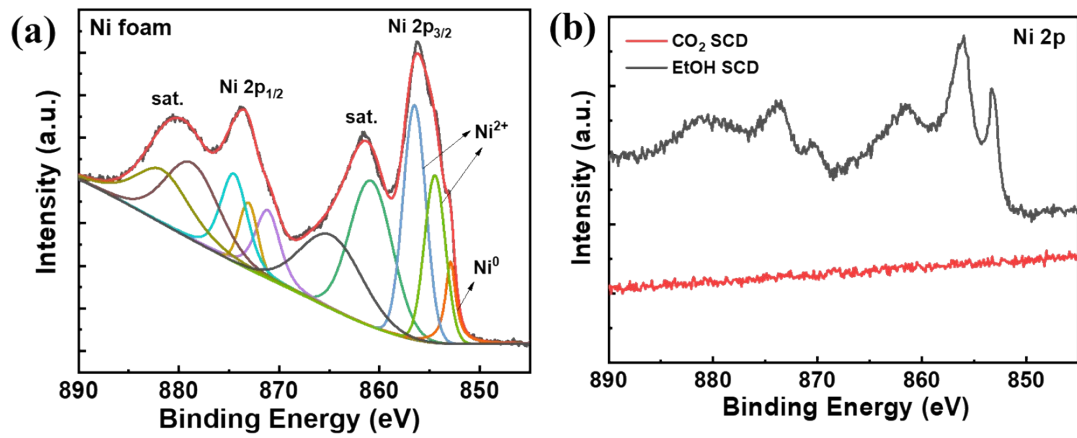


Figure S11. XPS Ni 2p spectra of (a) acid treated NF and (b) CO₂ supercritical dried (60 °C, 130 bar) and EtOH supercritical dried of as-synthesized samples.

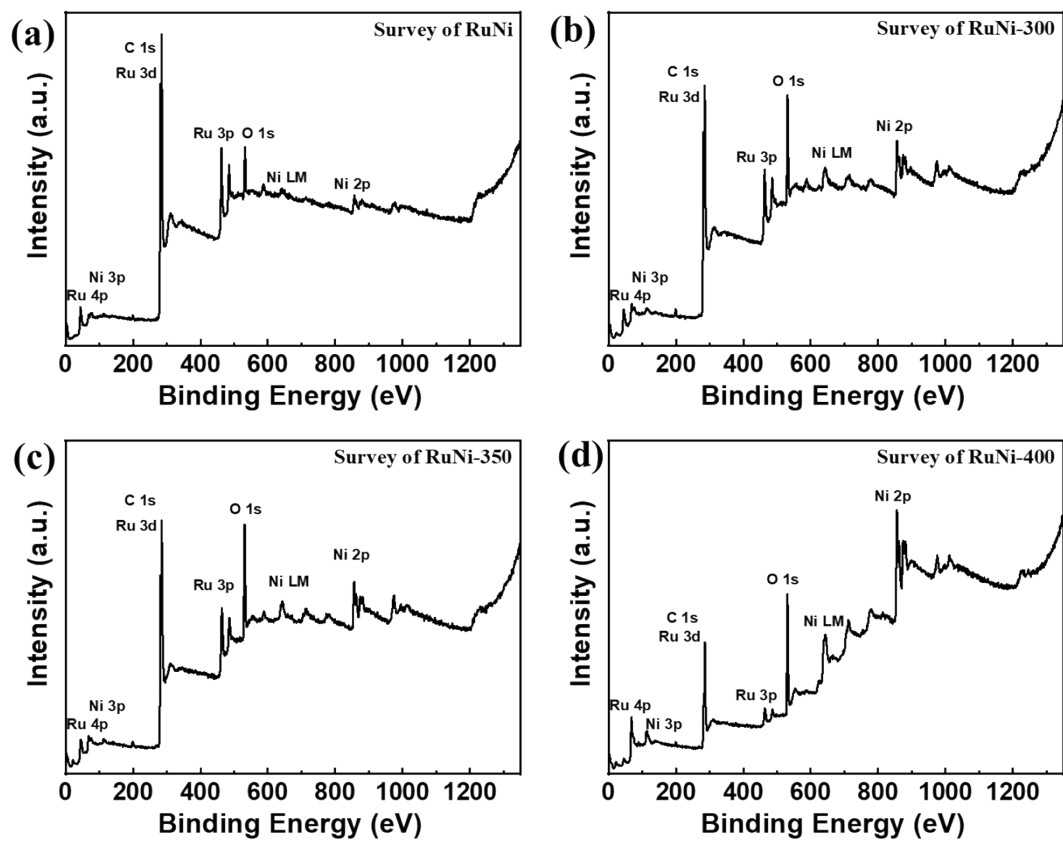


Figure S12. XPS survey scan of (a) RuNi, (b) RuNi-300, (c) RuNi-350, and (d) RuNi-400 aerogels.

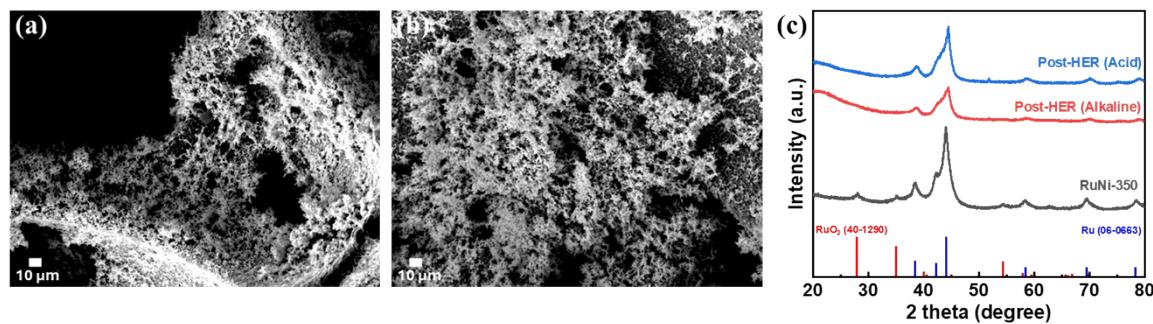


Fig. S13. SEM images of the RuNi-350@NF electrocatalysts after long-term (35 h) stability test (a) alkaline and (b) acidic electrolyte. The comparison analyses of (c) XRD patterns for before and after the long-term stability tests.

Table S5. Electrolyte analyses using inductively coupled plasma-mass spectrometry (ICP-MS) after the stability test

Element	Ni [ppb(ng/mL)]	Ru [ppb(ng/mL)]	Pt [ppb(ng/mL)]
Alkaline (KOH)	0.274	2.015	not detected
Acidic (H₂SO₄)	1663.547	26.822	not detected

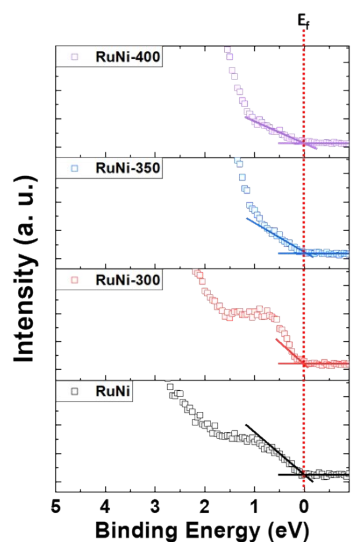


Figure S14. Valence band spectra of RuNi, RuNi-300, RuNi-350, and RuNi-400 aerogel samples with the E_f obtained from reference metallic gold.

Table S6. Comparison of the electrocatalytic HER activity of various Ru-based catalysts in both alkaline and acidic electrolytes

Catalysts	Alkaline (1 M KOH)		Acid (0.5 M H ₂ SO ₄)		References
	Overpotential at 10 mA·cm ⁻² (mV)	Tafel slope (mV·dec ⁻¹)	Overpotential at 10 mA·cm ⁻² (mV)	Tafel slope (mV·dec ⁻¹)	
RuNi-350@NF	51 (89@50, 117@100)	34.0	21 (61@50, 94@100)	30.9	This work
Ru-Ru ₂ P-4	18	30.2	58	34.8	InfoMat, 4 (2022) e12287
Ru/Ni ₃ NNi	53	32.4	-	-	Chem. Comm., 56 (2020) 2352
Ru-NG	25.9	32.6	~90	55.9	Carbon, 183 (2021) 362
Ru@Co/N-CNTs	48	33	92	30	ACS Sustainable Chem. Eng., 8 (2020) 9136
RuO ₂ -300Ar	17	35	16	-	Energy Environ. Sci., 14 (2021) 5433
Ru-MnFeP/NF	35	36	-	-	Adv. Energy Mater., 10 (2020) 2000814
Ru@C ₂ N	17	38	13.5	30	Nat. Nanotechnol., 12 (2017) 441
CoRu _{0.5} /CQDs	18	38.5	-	-	Angew. Chem. Int. Ed., 60 (2021) 3290
Ru@WNO-C	24	39.7	172	38.9	Nano Energy, 80 (2021) 105531
Ru@Ni-MOF	22	40	~60	33	Angew. Chem. Int. Ed., 60 (2021) 22276
RuNi/CQDs-600	13	40	58	55	Angew. Chem. Int. Ed., 59 (2020) 1718
CNT-V-Fe-Ru	38	41	64	51	ACS Catal., 13 (2023) 49
RuP/H-NC-900	19	42	76	-	Nanotechnology, 31 (2020) 295401
Ru-NiCoP/NF	44	45.4	-	-	Appl. Catal. B, 279 (2020) 119396
Ru/NC-400	39	49	55	40	Adv. Funct. Mater., 31 (2021) 2100698
MiSC-1	12	50	49	43	Adv. Energy Mater., 11 (2021) 2100141
Ru@CN	35	53	126	-	Energy Environ. Sci., 11 (2018) 800
ECM@Ru	83	59	63	47	Adv. Energy Mater., 10 (2020) 2000882
Ru/Ni-V ₂ NO/NCNFs	74.5	60.7	-	-	J. Electroanal. Chem., 911 (2022) 116213
a-Ru@Co-DHC	40	62	-	-	Chin. J. Catal., 43 (2022) 110
Ru _{0.10} @2H-MoS ₂	51	64.9	168	77.5	Appl. Catal. B, 298 (2021) 120490
RuP ₂ @NPC	52	69	38	38	Angew. Chem. Int. Ed., 56 (2017) 11559
CoRuO/A@HN C-2	85	72.5	-	-	ACS Appl. Mater. Interfaces, 12 (2020) 51437
Ru SAs-Ni ₂ P	57	75	125	71	Nano Energy, 80 (2021) 105467

Ru-Mo ₂ C/CN	34	80	-	-	J. Catal., 392 (2020) 313
Ru-NiFe-P	44	80	-	-	Appl. Catal. B, 263 (2020) 118324
S-RuP@NPSC	92	90.23	-	-	Adv. Sci., 7 (2020) 2001526
Ru-SA/Ti ₃ C ₂ T _x	-	-	70	27.7	Small, 16 (2020) 2002888
Ru-modified FeP	-	-	62	45	J. Mater. Chem. A, 8 (2020) 22607